LA-UR -91-825

LA-UR--91-825

DE91 009944

Los Alamos National Laboratory is operated by the University of California for the United States Department of Energy under contract W-7405-ENG-36

TITLE APPLICATION OF A THREE-DIMENSIONAL, PROGNOSTIC MODEL TO MEXICO CITY AIR QUALITY STUDIES

AUTHOR(S) M. D. Williams, and W. M. Porch

SUBMITTED TO 84th Annual Mtg. of the Air and Waste Management Assoc., Vancouver, Canada June 16-21, 1991

DISCLAIMER

Los Alamos Los Alamos National Laboratory
Los Alamos, New Mexico 87545

Abstract Form

Paper number 91-85.8

Author's name Michael D. Williams and William Porch

Type your abstract in the box below.

91-85.8

Application of a Three-Dimensional, Prognostic Model to Mexico City Air Quality Studies

Los Alamos National Laboratory and Instituto Mexicano del Petroleo have embarked on a joint study of options for improving air quality in Mexico City. One of the first steps in the process is to develop an understanding of the existing air quality situation. In this context we have begun by modifying a three-dimensional, prognostic, higher order turbulence model for atmospheric circulation (HOTMAC) to treat domains which include an urbanized area. This sophisticated meteorological model is required because of the complexity of the terrain and the relative paucity of meteorological data. The basic model (HOTMAC) was modified to include an urban canopy and urban heat sources. HOTMAC has been used to drive a Monte-Carlo kernel dispersion code (RAPTAD). RAPTAD was used to model the flow of carbon monoxide and sulfur dioxide, and the results have been compared to measurements. In addition the modeled wind fields which are based on upper-level winds from the airport are compared to the measured low-level winds. Also, a four year history of temperature structure obtained from the rawinsode at the airport has been related to mixing parameters and less reactive pollutant measurements (such as carbon monoxide)

Excess Page Charge Form

Because my paper exceeds 16 pages (including the title page, text, figures, and tables), I agree to pay an excess page fee to the Air & Waste Management Association.

Signed

Date

91-85.8

Application Of a Three-Dimensional, Prognostic Model to Mexico City Air Quality Studies

Michael D. Williams
Los Alamos National Laboratory
Group A-4
Mail Stop B299
Los Alamos, NM 87545

William Porch
Los Alamos National Laboratory
Group EES-5
Mail Stop D466
Los Alamos, NM 87545

March 1, 1991

INTRODUCTION

Los Alamos National Laboratory and Insituto Mexicano del Petroleo have embarked on a joint study of options for improving air quality in Mexico City. One of the first steps in the process is to develop an understanding of the existing air quality situation. The intent is to develop a modeling system which can address the behavior of pollutants in the region so that options for improving Mexico City air quality can be properly evaluated. The focus of the early efforts is to learn what we can from the data which has been collected in the past. The project is currently conducting a field program which will yield a variety of data which can be used to further evaluate and improve the models.

Initially, we are concentrating on meteorological variables and the behavior of carbon monoxide and sulfur dioxide. While ambient standards are sometimes violated for carbon monoxide and sulfur dioxide; violations are not as frequent for these pollutants as they are for others such as photochemical oxidants. However, the intent is to use CO and SO2 to help us understand the factors which govern dispersion before we add the additional complexity of chemistry.

In addition, critical elements of the emission inventory needed for the photochemistry are not yet available. We have begun by examining the relationship between CO and mixing depth and by modifying a three-dimensional, prognostic, higher order turbulence model for atmospheric circulation (HOTMAC) to treat domains which include an urbanized area. The sophisticated meteorological model is required because of the complexity of the terrain and the relative paucity of meteorological data.

Mexico City lies at an elevation of approximately 7500 feet above sea level in a "U" shaped basin which opens to the north. Mountains on the east and southeast sides of the basin reach elevations in excess of 17,000 feet. The city occupies a major part of the southwest portion of the basin. Upper level winds are provided by rawinsondes at the airport, low-level winds are measured at several sites within the city. Many of the sites have obstructed upwind fetches for a variety of directions.

During the wintertime when the worst air quality is measured, the winds are frequently light, and out of the northeast. This means the winds are light within the city, but significant slope winds develop which influence the behavior of the pollutants. The result of this combination of circumstances is a relatively short-residence time for morning rush-hour emissions, but a

long residence-time for afternoon and evening emissions.

The basic model (HOTMAC) was modified to include an urban canopy and urban heat sources. HOTMAC is used to drive a Monte-Carlo kernel dispersion code (RAPTAD). Also, a four year history of temperature structure obtained from the rawinsonde at the airport has been related to mixing parameters and less reactive pollutant measurements (such as carbon monoxide).

THE METEOROLOGICAL MODELING SYSTEM

Model Formulation

HOTMAC is a three-dimensional time-dependent model developed by T. Yamada[1]. It uses the hydrostatic approximation and a terrain following coordinate system in which the vertical coordinate z^*, is given by:

$$z^* = \tilde{H}\frac{z - z_g}{H - z_g} \tag{1}$$

where z_g is the height of the ground and H is the height of the top of model domain. $\tilde{H}$ is equal to H minus the height of the highest terrain in the domain.

HOTMAC solves conservation relations for the horizontal wind components, potential temperature, moisture, turbulent kinetic energy, and the turbulence length scale. HOTMAC describes advection, coriolis effects, turbulent transfer of heat, momentum, and moisture. It also describes solar and terrestrial radiation effects, turbulent history effects, and drag and radiation effects of forest canopies.

Equation 2 represents the conservation equation for the east-west component of momentum. The total rate of change of the u component of the wind is equal to the sum of a coriolis term, a buoyancy term, two horizontal eddy transport terms and a vertical momentum transport term.

$$\frac{DU}{Dt} = f(V - V_g) + g\frac{\tilde{H} - z^*}{\tilde{H}}\left(1 - \frac{\langle\Theta_v\rangle}{\Theta_v}\right)\frac{\partial z_g}{\partial x} \tag{2}$$

$$+\frac{\partial}{\partial x}\left(K_x\frac{\partial U}{\partial x}\right)+\frac{\partial}{\partial y}\left(K_{xy}\frac{\partial U}{\partial y}\right)+\frac{\overline{H}}{H-z_g}\frac{\partial}{\partial z^*}(-\overline{uw}).$$

V_g is the north-south component of the geostrophic wind. $\langle\theta_v\rangle$ is the horizontal average of the virtual potential temperature. Equation 3 is a similar expression for the north-south components of momentum.

$$\frac{DV}{Dt}=-f(U-U_g)+g\frac{\overline{H}-z^*}{\overline{H}}\left(1-\frac{\langle\Theta_v\rangle}{\Theta_v}\right)\frac{\partial z_g}{\partial y} \tag{3}$$
$$+\frac{\partial}{\partial x}\left(K_{xy}\frac{\partial V}{\partial x}\right)+\frac{\partial}{\partial y}\left(K_y\frac{\partial V}{\partial y}\right)+\frac{\overline{H}}{H-z_g}\frac{\partial}{\partial z^*}(-\overline{vw}).$$

Equation 4 is derived from the hydrostatic approximation and it describes the vertical velocity W^*, in the z^* coordinate system.

$$\frac{\partial U}{\partial x}+\frac{\partial V}{\partial y}+\frac{\partial W^*}{\partial z^*}-\frac{1}{H-z_g}\left(U\frac{\partial z_g}{\partial x}+V\frac{\partial z_g}{\partial y}\right)=0. \tag{4}$$

Equation 5 is the energy conservation equation which describes the total rate of change of the potential temperature.

$$\frac{D\Theta}{Dt}=\frac{\partial}{\partial x}\left[K_x\frac{\partial\Theta}{\partial x}\right]+\frac{\partial}{\partial y}\left[K_y\frac{\partial\Theta}{\partial y}\right]+\frac{\overline{H}}{H-z_g}\left[\frac{\partial}{\partial z^*}(-\overline{w\theta})+\frac{1}{\rho C_p}\frac{\partial R_N}{\partial z^*}\right]. \tag{5}$$

The last two terms are the contributions from divergence of the sensible heat flux and divergence of the radiation field. R_N is the long wave radiation flux.

Equation 6 describes the conservation of moisture mixing ratio.

$$\frac{DQ_v}{Dt}=\frac{\partial}{\partial x}\left[K_x\frac{\partial Q_v}{\partial x}\right]+\frac{\partial}{\partial y}\left[K_y\frac{\partial Q_v}{\partial y}\right]+\frac{\overline{H}}{H-z_g}\frac{\partial}{\partial z^*}(-\overline{wq_v}). \tag{6}$$

An important difference between the higher order turbulence models such as this one and simpler models is the treatment of turbulent fluxes, described by Equations 7 and 8.

$$\overline{uw}=-lqS_M\frac{\partial U}{\partial z}. \tag{7}$$

$$\overline{w\theta}=-\alpha lqS_H\frac{\partial\Theta}{\partial z}. \tag{8}$$

The turbulent fluxes involve two other factors: l, and q in addition to the gradients and the factor $\tilde{S}_M$ which is a function of the flux Richardson number. Simpler models would use some form of the latter two factors, but not q, the turbulence speed or l which is the turbulence length scale. q and l are obtained by solving Equations 9 and 10.

$$\frac{D}{Dt}\left(\frac{q^2}{2}\right) = \frac{\partial}{\partial x}\left[K_x\frac{\partial}{\partial x}\left(\frac{q^2}{2}\right)\right] + \frac{\partial}{\partial y}\left[K_y\frac{\partial}{\partial y}\left(\frac{q^2}{2}\right)\right] + \left(\frac{\overline{H}}{H-z_g}\right)^2\frac{\partial}{\partial z^*}\left[q\mathbf{l}S_q\frac{\partial}{\partial z^*}\left(\frac{q^2}{2}\right)\right] - \frac{\overline{H}}{H-z_g}\left(\overline{uw}\frac{\partial U}{\partial z^*} + \overline{vw}\frac{\partial V}{\partial z^*}\right) + \beta g\overline{w\theta_v} - \frac{q^3}{B_1\mathbf{l}}. \tag{9}$$

$$\frac{D}{Dt}(q^2\mathbf{l}) = \frac{\partial}{\partial x}\left[K_x\frac{\partial}{\partial x}(q^2\mathbf{l})\right] + \frac{\partial}{\partial y}\left[K_y\frac{\partial}{\partial y}(q^2\mathbf{l})\right] + \left(\frac{\overline{H}}{H-z_g}\right)^2\frac{\partial}{\partial z^*}\left[q\mathbf{l}S_1\frac{\partial}{\partial z^*}(q^2\mathbf{l})\right] + \mathbf{l}F_1\left[\frac{\overline{H}}{H-z_g}\left(-\overline{uw}\frac{\partial U}{\partial z^*} - \overline{vw}\frac{\partial V}{\partial z^*}\right) + \beta g\overline{w\theta_v}\right] - \frac{q^3}{B_1}\left[1 + F_2\left(\frac{\mathbf{l}}{kz}\right)^2\right]. \tag{10}$$

The development of these equations and form of the factors is described by Yamada[3] and Mellor and Yamada[4].

Within the soil, Equation 11 applies:

$$\frac{\partial T_s}{\partial t} = \frac{\partial}{\partial z_s}\left(K_s\frac{\partial T_s}{\partial z_s}\right). \tag{11}$$

A key feature of the model is its description of the surface energy budget Equation 12.

$$R_s + R_L\downarrow - R_L\uparrow = H_s + LE + G_s. \tag{12}$$

R_s is the solar shortwave radiation flux, while $R_L\downarrow$ is the downward long wave atmospheric flux and $R_L\uparrow$ is the blackbody radiation from the surface. The sensible heat flux H_s, is given by:

$$H_s = -\rho_a c_p u^*\theta^*. \tag{13}$$

where u^* is the friction velocity and θ^* is a temperature scale which is defined by:

$$\theta^* = \frac{k}{P_r} \frac{(\Theta(z_1) - \Theta_G)}{\left[In\left(\frac{z_1 + z_{oh}}{z_o}\right) + In\left(\frac{z_o}{z_1}\right) - \Psi\right]}. \tag{14}$$

In Equation 14, Ψ is a stability correction factor which is zero during neutral atmospheric stability. Similar expressions are used to define u^* except that velocity at the ground is zero. LE is the latent energy flux and G_s is the soil heat flux. Equations 15 and 16 describe these variables.

$$LE = \rho_a L u^* Q^*. \tag{15}$$

$$G_s = -K_s \frac{\partial T_s}{\partial z_s}|_G. \tag{16}$$

In an urban context the surface energy balance requires an additional term which represents the heat released by man's activities. The additional heat along with differences in thermal properties between urban and non-urban surfaces produces the urban heat island.

Meteorological Model Application

HOTMAC requires both terrain and meteorological inputs. The model begins with a temperature field which is horizontally uniform. Initial potential temperatures are derived from the potential temperature at sea level and the potential temperature gradients below the height of the point which is being initialized. The vertical potential temperature is idealized as composed of up to three line segments which are continuous but have different slopes.

Three days in which air quality was poor, good, and normal were chosen for detailed modeling. All of the days were in winter of 87-88. Meteorological inputs were based on the afternoon rawinsonde of the preceding days which was used to estimate synoptic scale wind and temperature profiles. The bad day (2-4-1988) featured light winds out of the north-northeast. The normal day had moderate winds from the north-northwest. The good day had high winds (9 meters per second) out of the southwest. We used a nested grid system to model the valley of Mexico and its surrounding terrain. The outer grid has a 6 km spacing and covers the major terrain influences as shown in Figure 1. The inner grid as shown in Figure 2 embraces the city and the immediately adjacent slopes. It has a grid size of 2 km.

The urban canopy was approximated by using the estimated distribution of CO emissions defined on a 1 km grid. The relative CO emissions were used to proportion the fraction of the area of a grid cell which was covered by canopy (roof tops), the average soil conductivity, average soil heat capacity, and the urban heat release intensity. For example, in the cells with the highest CO emissions the fraction area of the canopy within the cell would be set to 0.75, while soil conductivity and heat capacity would be chosen to represent pavement. For areas with low emissions the canopy fractions would be set to .20 and the soil parameters would be more nearly those of soil. The heat release was estimated based on the energy released by automobiles when emitting the specified levels of CO. The urban heat release reached 35 watts per square meter in some areas. Many of the parameters used to represent the urban canopy are first estimates which will be refined as more information on land use and urban skin temperatures becomes available during the course of the study.

THE PARTICLE TRANSPORT CODE RAPTAD

Model Formulation

RAPTAD is a Monte Carlo random particle statistical diffusion code, developed by Ted Yamada[5]. Pseudo-particles are transported with instantaneous velocities that include the mean wind field and the turbulence velocities. The turbulence velocity is generated randomly consistent with the standard deviation of the wind at the particle location. The location of each pseudo-particle represents the center of mass of a concentration distribution for each puff. The total concentration at any point is obtained by adding the concentration contributions of each puff at that point (a kernel method).

Other particle transport codes produce concentrations by counting particles within a sampling volume. The computed concentration level could vary considerably depending upon the size of the sampling volume and number of particles used in the computation. For example, if the sampling volume is very small, the concentration distribution becomes excessively variable in space. On the other hand, if the sampling volume is too large, the concentration distribution will be over smoothed. The kernel method avoids this difficulty and provides smooth concentration distributions with relatively few particles.

The first step is to calculate the positions and turbulence history of a group of pseudo-

particles that represent the emissions from a release. Locations of particles are computed from:

$$x_i(t + \Delta t) = x_i(t) + U_{pi}\Delta t \tag{17}$$

where

$$U_{pi} = U_i + u_i \tag{18}$$

$$u_i(t + \Delta t) = au_i(t) + b\sigma_{u_i}\zeta + \delta_{i3}(1 - a)t_{Lx_i}\frac{\partial}{\partial x_i}(\sigma_{u_i}{}^2) \tag{19}$$

$$a = \exp\left(-\frac{\Delta t}{t_{Lx_i}}\right) \tag{20}$$

and

$$b = (1 - a^2)^{1/2} \tag{21}$$

In the above expressions U_{pi} is the particle velocity in the x_i direction, U_i is the mean velocity, u_i is the turbulence velocity, ζ is a random number from a Gaussian distribution with zero mean and unit variance, t_{Lx_i} is the Lagrangian integral time scale for the velocity u_i, σ_{u_i} is the variance of the velocity fluctuation u_i, and δ_{i3} is the Dirac delta. The last term on the right hand side of Equation 19 was introduced by Legg and Raupach[6] to prevent the accumulation of particles in low-energy areas. The mean velocity U_i and vertical velocity variance σ_i are obtained from the output of HOTMAC.

The Monte Carlo kernel method requires that a functional form for the distribution kernel be chosen and that parameters that describe the width, breadth, and depth of the distribution be calculated. Various functional forms can be assumed to express the concentration distribution in the puff. One of the simplest ways is to assume a Gaussian distribution where variances are determined as the time integration of the velocity variances encountered over the history of the puff. The concentration level at a given time and space is determined as the sum of the concentrations each puff contributes. The concentration χ at (X, Y, Z) is estimated by using the following expression:

$$\chi(X, Y, Z) = \frac{Q\Delta t}{(2\pi)^{3/2}}\sum_{k=1}^{N}\frac{1}{\sigma_{x_k}\sigma_{y_k}\sigma_{z_k}}\exp\left(-\frac{1}{2}\frac{(X_k - X)^2}{\sigma_{x_k}{}^2}\right) \tag{22}$$

$$\bullet\exp\left(-\frac{1}{2}\frac{(y_k - Y)^2}{\sigma_{y_k}{}^2}\right)$$

$$\bullet\left\{\exp\left(-\frac{1}{2}\frac{(z_k - Z)^2}{\sigma_{z_k}{}^2}\right) + \exp\left(-\frac{1}{2}\frac{(z_k + Z - 2z_g)^2}{\sigma_{z_k}{}^2}\right)\right\}$$

where (x_k, y_k, z_k) is the location of the k^{th} particle; σ_{xk}, σ_{yk}, and σ_{zk} are standard deviations of a Gaussian distribution; and z_g is the ground elevation. The variances are estimated based on Taylor's homogeneous diffusion theory[7]. For example σ_y is obtained from

$$\sigma_y^2 = 2\sigma_v^2 \int_o^t \int_o^\zeta R(\zeta) d\zeta dt \tag{23}$$
$$= 2\sigma_v^2 t_{Ly} \left(t + t_{Ly} \exp\left(-\frac{t}{t_{Ly}} \right) - t_{Ly} \right)$$

where a correlation function $R(\zeta) = \exp\left(\frac{-\zeta}{t_{Ly}}\right)$ is used. Equation 23 is approximated by

$$\sigma_y = \sigma_v tt \leq 2t_{Ly} \tag{24}$$

and

$$\sigma_y^2 = 2t_{Ly}\sigma_v^2 tt > 2t_{Ly} \tag{25}$$

Although the turbulence field is not normally homogeneous, we assume the theory can be applicable over a short time period, such as an integration time step. Therefore,

$$\sigma_y(t + \Delta t) = \sigma_y(t) + \sigma_v \Delta tt \leq 2t_{Ly} \tag{26}$$

and

$$\sigma_y^2(t + \Delta t) = \sigma_y^2(t) + 2t_{Ly}\sigma_v^2 \Delta tt > 2t_{Ly} \tag{27}$$

are used. Similar relations are used for the x and z directions. The standard deviations σ_u, σ_v, and σ_w at each particle location are obtained by interpolating grid values of a computation grid volume in which a particle is located.

Model Application

Concentration predictions were carried out for each of the three days for both CO and SOx. Emissions on a 1 km x km grid were available. These cells were organized into a cumulative distribution of the total emissions. RAPTAD was modified so that it chose a random number

between 0 and 1 each time a pseudo-particle was to be released. The random number was used to define a point on the cumulative emission distribution and to select the emission cell which included that point on the distribution. The pseudo-particle was then released from the center of the cell. Each cell was given the same initial sigmas which were chosen to approximate the early plume growth resulting from sub-grid scale features. In the case of SOx emissions from point sources an initial plume height above the surface was chosen based on the emission rate for the cell. Ideally, this approximate approach will be replaced by detailed effective plume height calculations, however, the relevant details are not yet available. Both the CO and SOx emission characterizations will be improved by better data on time profiles and the spatial parameters.

EMPIRICAL STUDIES ON MIXING HEIGHT AND CO RELATIONSHIPS

Mixing height and stability parameters were studied for Mexico City using temperature profiles from rawinsonde launched from the Mexico City airport from 1985-1988. Rawinsondes were launched at 12 and 0 GMT (0600 and 1800 LST), and these have been labeled as morning and evening, respectively. The mixing depth is calculated from the potential temperature profile by determining the base of an elevated inversion using standard techniques[8]. However, often morning soundings, particularly in winter show a ground based inversion. Theoretically this situation should lead to no vertical mixing. However, studies in the San Francisco Bay area[9] and in a basin near a power plant[10] show that pollutants do mix to the top and bottom of a ground based inversion. How this occurs is not well understood, however, terrain effects, basin waves induced by shear and initial plume buoyancy effects may all play a role. Therefore, we have also taken a depth of a ground based inversion as the mixing height when this occurs.

The ultimate test of the importance of mixing height to air pollution episodes is a direct comparison of mixing height history with pollution measurements. The best choice for this comparison is visibility because it represents an integrated property which is more likely to be affected by large scale accumulation due to low mixing heights. However, we haven't yet obtained visibility data from Mexico City. The next best choice is carbon monoxide which has little chemical and photochemical reactivity. Figure 3 shows a comparison of CO concentrations and mixing heights for January and February of 1988. For these purposes

a calculated mixing height of over 2 km was replaced by a value of 2 km because the concentrations are determined by other factors when mixing heights exceed 2 km. The CO data represent 1 hour averages of CO concentrations beginning at 0600 LST from the monitoring station closest to the airport. The mixing heights are determined from the morning rawinsonde profile.

Figure 4 reports similar data for a station on the northwest side of the city; the airport is on the east central side of the city. The two Figures show a general association of high CO concentrations with low mixing heights.

COMPARISON OF MODEL RESULTS AND OBSERVATIONS

Wind Predictions

Figures 5 and 6 depict the wind fields predicted by the model for the bad day (julian day 35) for 6am and 2 pm cst respectively. The additional wind vectors between those at the grid point are the measurements. In Figure 5 there are a total of six measurements including that of Station G which is separately marked. Station G is located on a hill and may not represent the 10 meter height winds calculated by the model. Figure 7 reports the model predictions for the vertical profiles at the grid point closest to station G. Figures 8 and 9 depict the wind fields on the normal day (December 7, 1987) at 6 am and 2 pm respectively. Finally, Figures 10 and 11 report the predicted and observed winds on the good day (January 24, 1988). The plots show only the situations where measurements of both the wind speed and the wind direction were available at a site. In many instances the wind directions were available while the wind speeds were missing which is to be expected for the low winds in the basin. The data from stations with higher winds may represent sites which are outside the urban canopy. The wind directions represent a larger data set. Figures 12 and 13 display the hourly winds at station T which is near the southwest corner of the city and at station Y which is near the airport on the eastern side of the city. For cases in which the measured wind is more than 180 degrees larger than the predicted wind, 360 degrees has been added to the predicted wind and vice versa for the opposite case. This adjustment is logical, but it does exaggerate the agreement between the model predictions are the observed winds.

Overall the a best-fit regression of the observed winds versus the predicted wind directions gave a slope of .95 with a correlation coefficient of .83 on the bad day. The standard error of the slope was .047 and the mean predicted wind was 172 degrees while the mean observed wind was from 204 degrees.

For data from all three days the relationship was much worse. In fact on 12/7 there was no significant correlation. Overall the data set gave a slope of 1.008 with a standard error of the slope of .04 and a correlation coefficient of 0.71. The mean measured wind direction was 247 degrees while the mean predicted wind direction was 222 degrees.

The modeling shows promise particularly for the days with strong local terrain forcing such as the bad day. However, there is much room for improvement. It also appears that the heat island may be overestimated. This would account for the poor performance on the good day when the model predicted that the combination of the large scale winds and the heat island was sufficient to overcome the local slope winds. The result was that the observed winds turned around in the afternoon while the modeled winds failed to do so. On the bad day the modeled winds turned around slower than the observed winds in the morning and faster in the evening.

Another aspect of the model application is the representation of the synoptic scale wind. In the applications to date the synoptic scale wind has been estimated from the rawinsonde of the previous afternoon. It is likely that there were changes in the synoptic scale wind during the model period (about 30 hours) during the normal day. In addition, the afternoon sounding was represented in a very simplified fashion in this application.

There are several aspects of the problem which will be examined in more detail during the next phase of the project when more detailed measurements become available. The measurements will provide skin temperatures, more vertical profiles, and better information on pollutant mixing. These measurements will allow us to improve the model's representation of the atmosphere in the region.

Modeled and Observed Concentrations

For the SOx predictions, the normal day showed the best correlation coefficient of .47 with a slope of 1.37 and nearly identical means of .036ppm predicted and .037ppm measured. On

the bad day the correlation coefficient was 0.2 with a slope of .24 and a predicted mean of .072 versus a measured mean of .030ppm. Overall the correlation coefficient was .22 with a slope of .34 and a predicted mean of .057ppm and a measured mean of .033ppm.

The CO comparisons showed no correlation for the good day with similar correlations for the bad and normal days. When the three days were lumped together the correlation coefficient was only 0.15 with a slope of .16. The mean predicted concentration was 5.0 ppm while the mean measured concentration was 3.8 ppm. Figure 14 reports the a comparison of the hourly predictions and measurements on the bad day for station A which had the highest single hour concentration. Figure 15 reports a similar comparison for station V which had the highest average concentration on the bad day.

Some of the model's performance deficiencies are probably the result of an inaccurate or insufficiently detailed description of the sources in the region. The fact that the soX predictions were much better on the windier day suggests that the fixed plume height for the sources was too low. A better description of the stacks and the plume rise associated with them is important. The CO performance could probably be improved by using a line source description for the major highways.

The model calculations indicated that the morning rush hour emissions escaped the urban area in a few hours. The evening emissions were initially transported up the slopes, but they were soon brought back into the domain as the downslope winds developed. In the simulations reported here we began the emissions at midnight, so that the model was not asked to describe the carry over emissions from the preceding evening. This deficiency in the application probably accounts for much of the discrepancy between the early morning predictions and measurements.

SUMMARY

A joint study of Mexico City's air quality problems between Los Alamos National Laboratory and the Instituto Mexicano Del Petroleo is underway. An early task was to examine existing ambient data and compare it to model predictions. The model uses a three-dimensional prognostic meteorological code to provide wind and turbulence fields to a Monte Carlo kernel, random particle transport code. A model of this sophistication was chosen because of the important terrain influences in the region and the limited meteorological data.

The modeling system was used to make predictions for three days with varying air quality Predictions were made and compared to experiments for winds and concentrations of CO and SOx. In addition a study of the measured mixing heights showed an association with mixing depths for days with low mixing heights

The modeling system shows promise for addressing the air quality questions, but there are also deficiencies in its application. Additional studies now underway will provide an opportunity to improve the model and the input data for this application.

ACKNOWLEDGMENTS

The authors are grateful to Dr. L. H. Auer for his assistance with data handling and display. They are also grateful to Dr. Javier Tejeda for providing important data and suggestions. The work is supported by the US Department of Energy and was performed under its auspices at Los Alamos National Laboratory.

REFERENCES

1. T. Yamada, "Numerical Simulation of the Night 2 Data of the 1980 ASCOT Experiments in the California Geysers Area," Archives for Meteorology, Geophysics, and Bioclimatology, Ser. A34, pp 223-247 (1985).

2. T. Yamada, "The Critical Richardson Number and the Ratio of the Eddy Transport Coefficients Obtained from a Turbulence Closure Model," J. Atmos. Sci., vol 32 pp926-933 (1975).

3. T. Yamada, "A Numerical Simulation of Nocturnal Drainage Flow," J. Meteor. Soc., Japan, vol 59, pp 108 122 (1981).

4. G. I. Mellor, and T. Yamada, "Development of a Turbulence Closure Model for Geophysical Fluid Problems," Rev. Geophys. Space Phys., vol 20, pp 851-875 (1982).

5. T. Yamada, and S. Bunker, "A Numerical Model Study of Nocturnal Drainage Flows with Strong Wind and Temperature Gradients," it J. Appl. Meteor., (submitted, 1988).

6. R. J. Legg and M. F. Raupach, "Markov-Chain Simulation of Particle Dispersion in Inhomogeneous Flows: The Mean Drift Velocity Induced by a Gradient in Eulerian Velocity Variance," Boundary-Layer Meteorol., vol 24 pp3-13 (1982).

7. G. I. Taylor, 1921: "Diffusion by Continuous Movements," Proceedings of the London Mathematical Society, Ser. **2**, vol 20 pp196-211 (1921).

8. R. F. Kelley, "User's Manual for Mixing Height Computer Program," U.S. Environmental Protection Agency, Research Triangle Park, NC, EPA-45014-81-022 (1981).

9. W. M. Porch, T. R. Galloway, T. J. Green, and H. W. Elleaesser, "Long Path Optical Extinction and Meteorology in the San Francisco Bay Area," Atmospheric Environment, vol. 15, pp 2555-2560 (1981).

10. W. D. Neff, "Remote Sensing of Atmospheric Processes Over Complex Terrain," Edited by W. Blumen, American Meteorological Society, Boston, MA, pp 209-217 (1990).

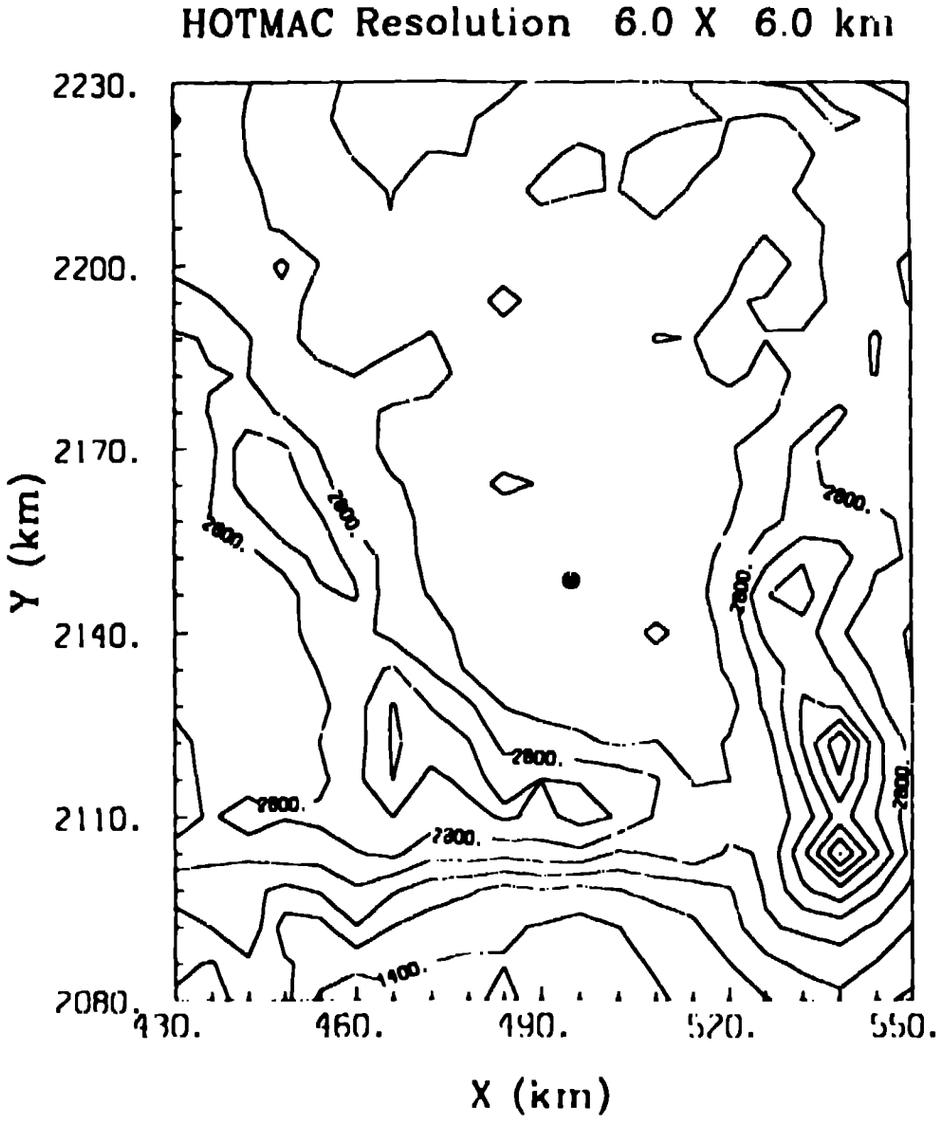

Figure 1: Coarse grid depiction of the model domain; the dot is the airport on the east side of the city. Contours are in meters.

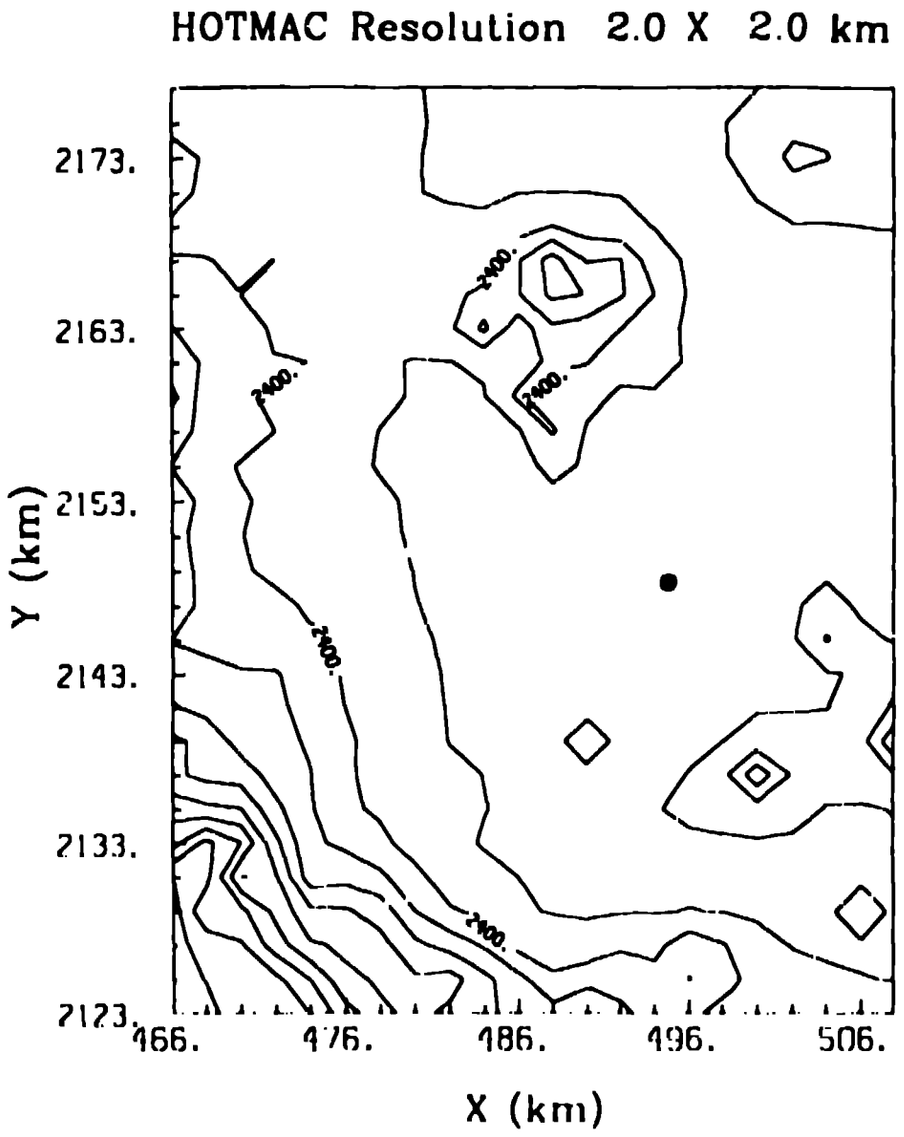

Figure 2 Fine grid depiction of the model domain; the dot is the airport on the east side of the city. Contours are in meters.

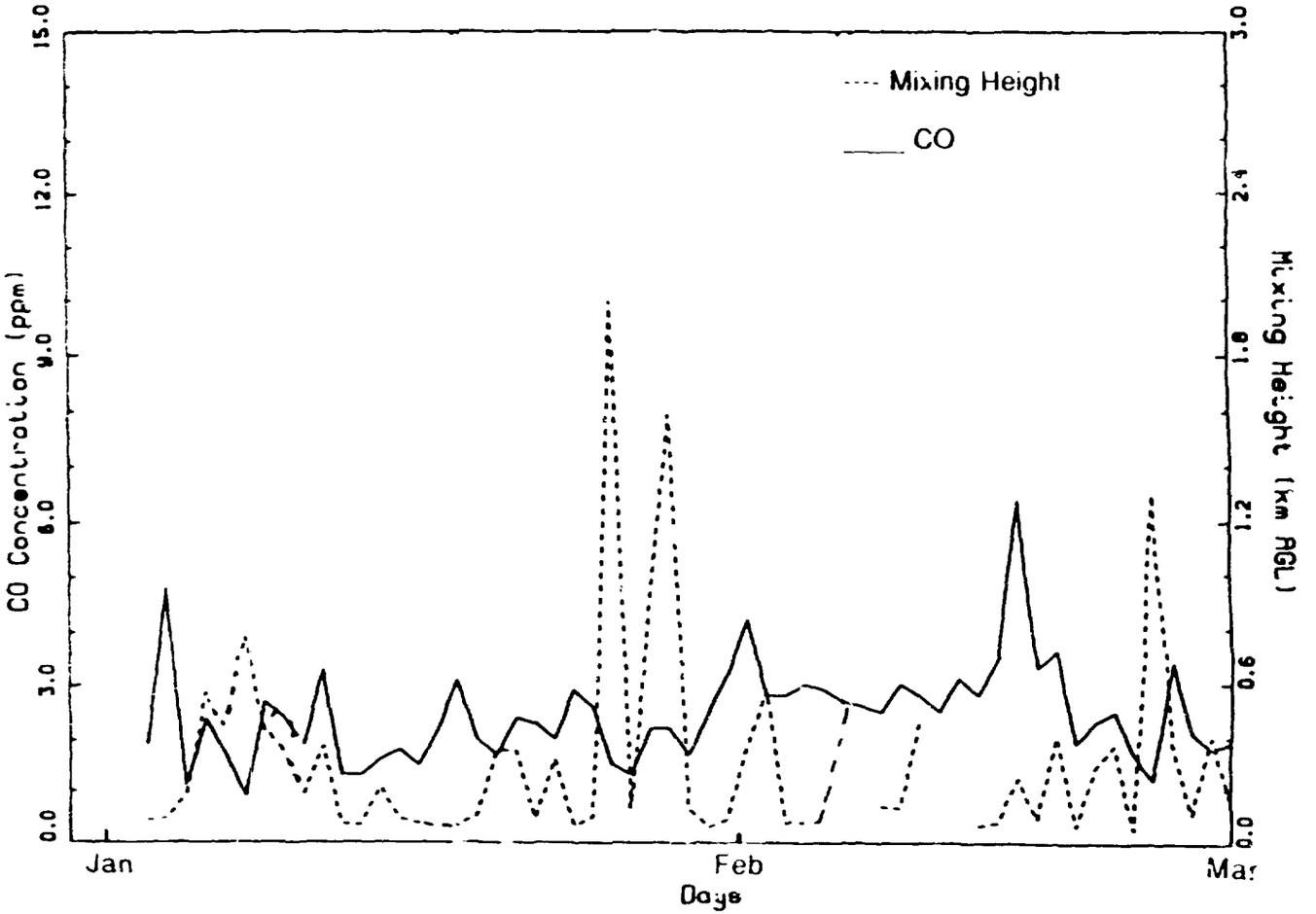

Figure 3. Mixing heights and co concentrations for the monitoring station nearest the airport

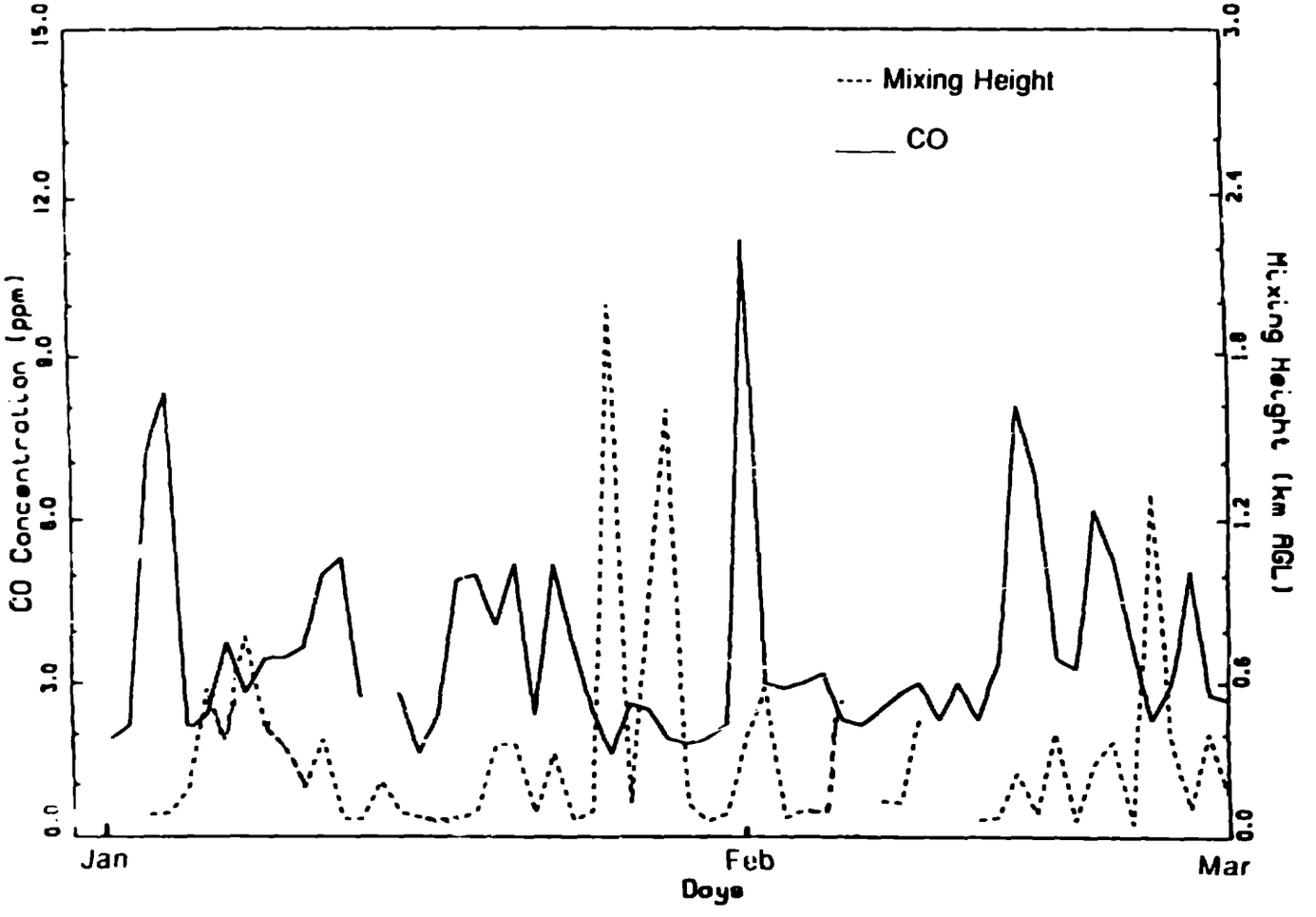

Figure 1: Mixing heights and co concentrations for the monitoring station on the northwest side of the city.

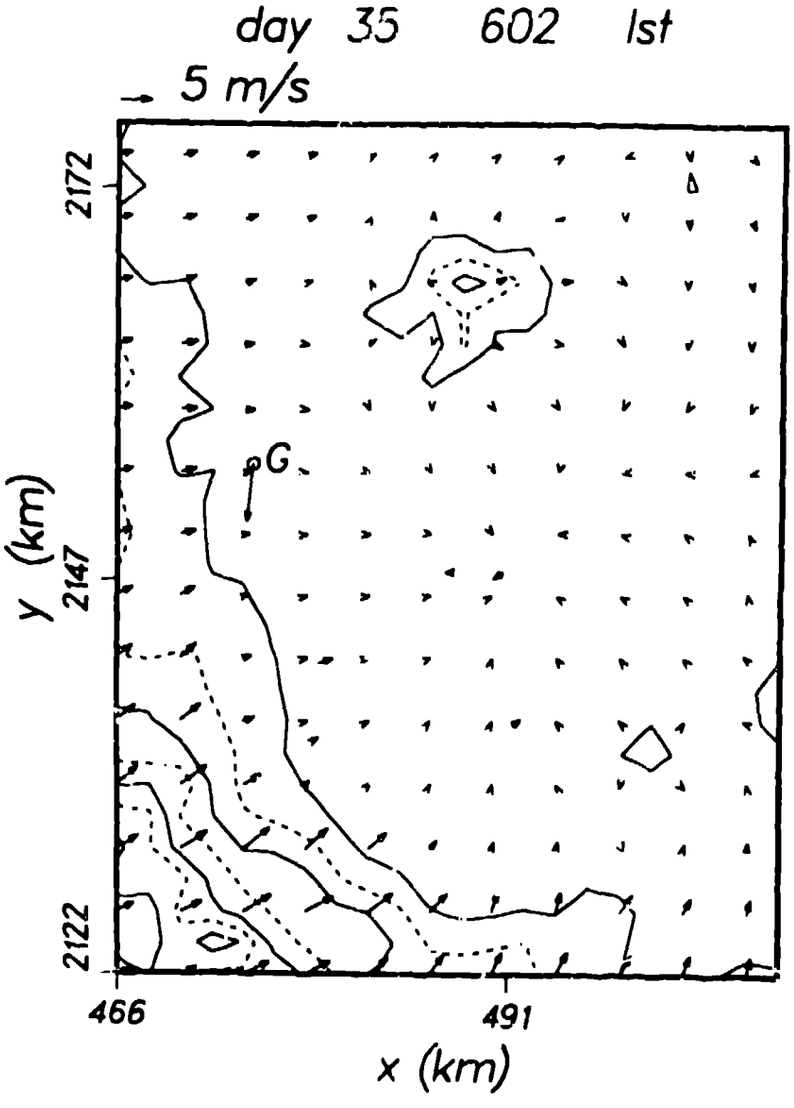

Figure 5: Modeled and measured 10 meter winds at 6 am on February 4 1988.

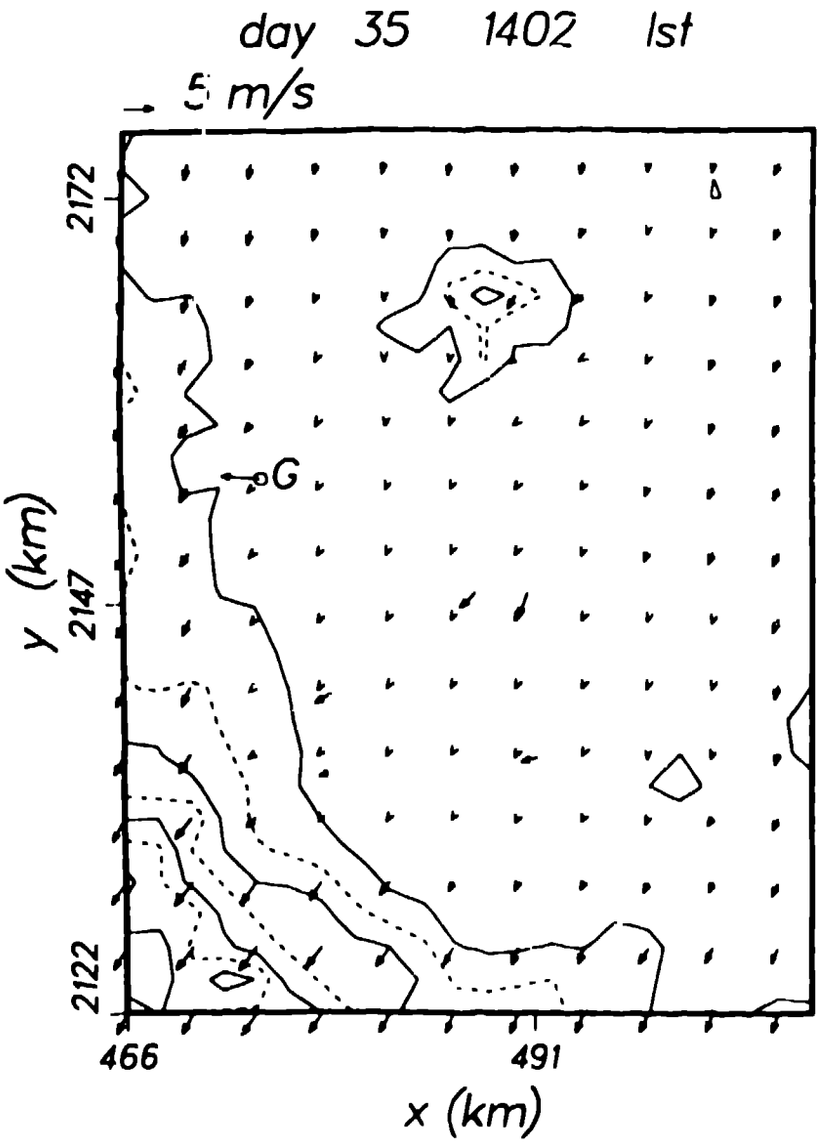

Figure 6: Modeled and measured 10 meter winds at 2 pm on February 4 1988.

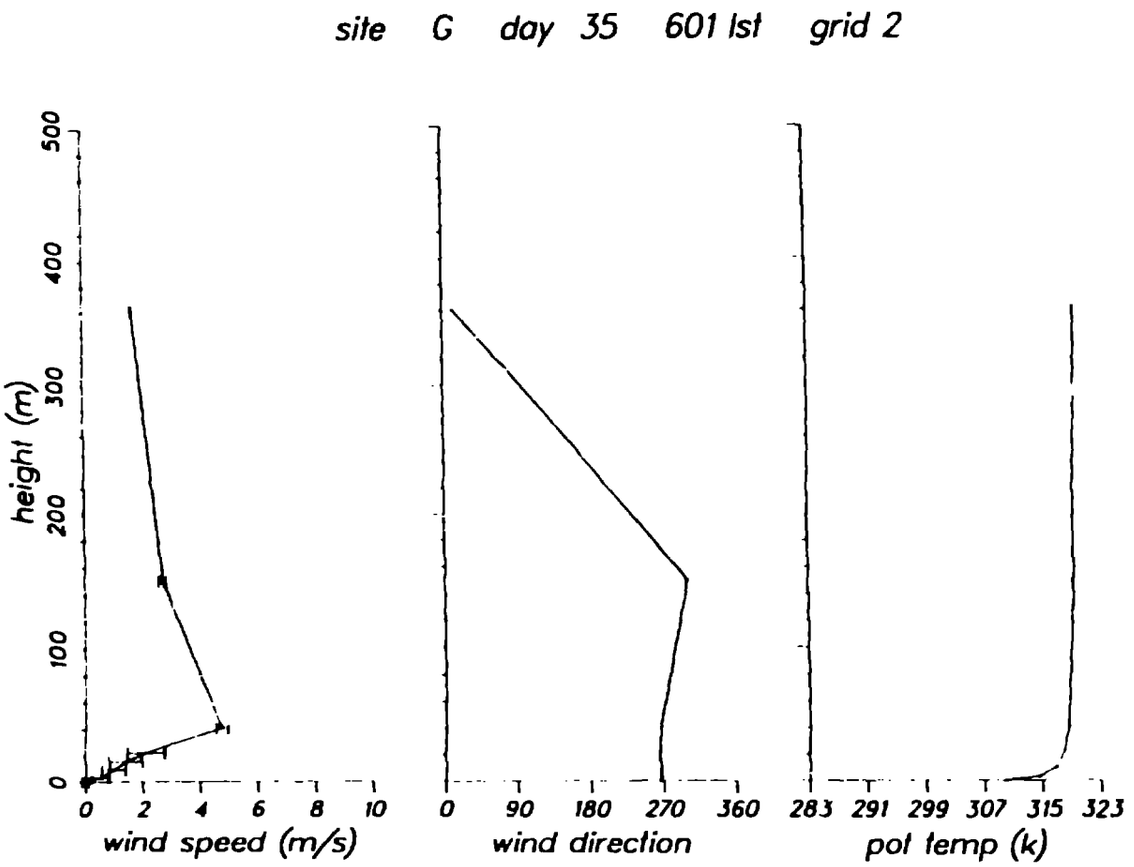

Figure 7: Modeled vertical wind and temperature profiles at G.

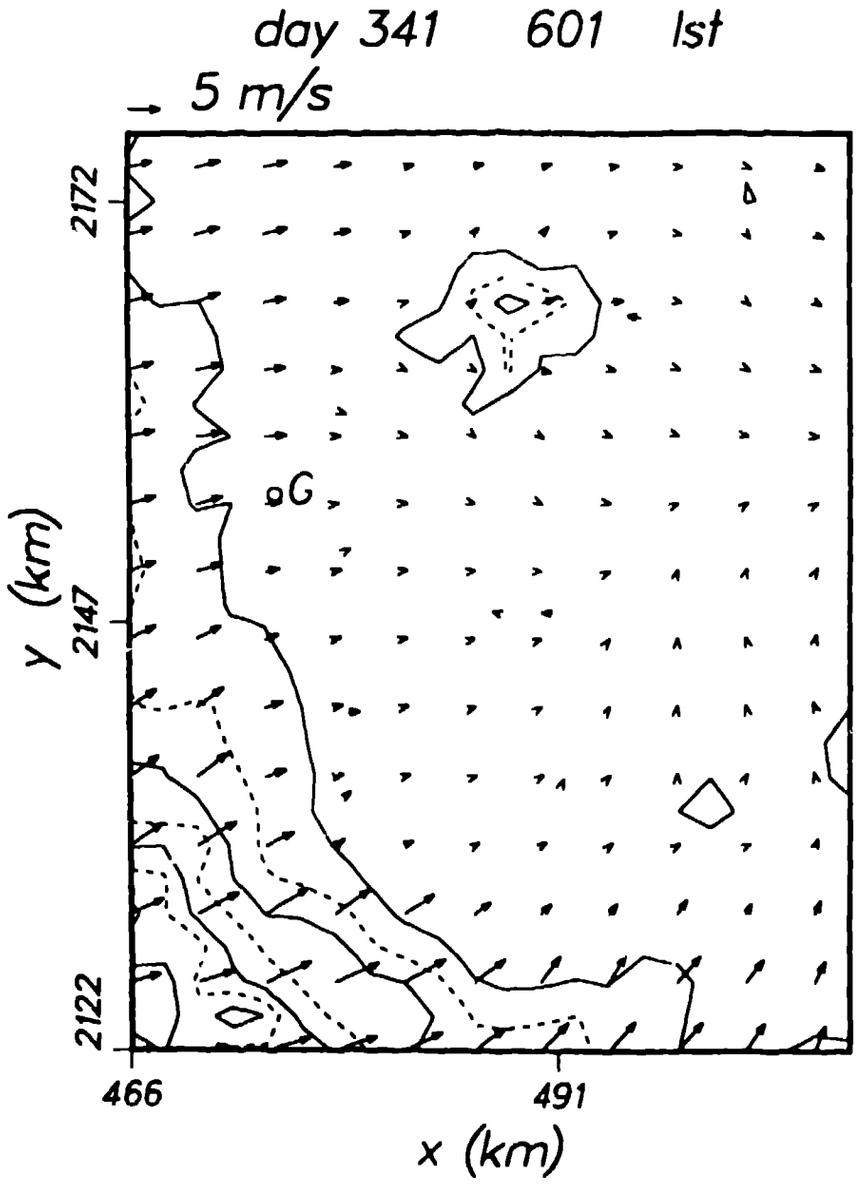

Figure 8: Modeled and measured 10 meter winds at 6 am on December 7, 1987.

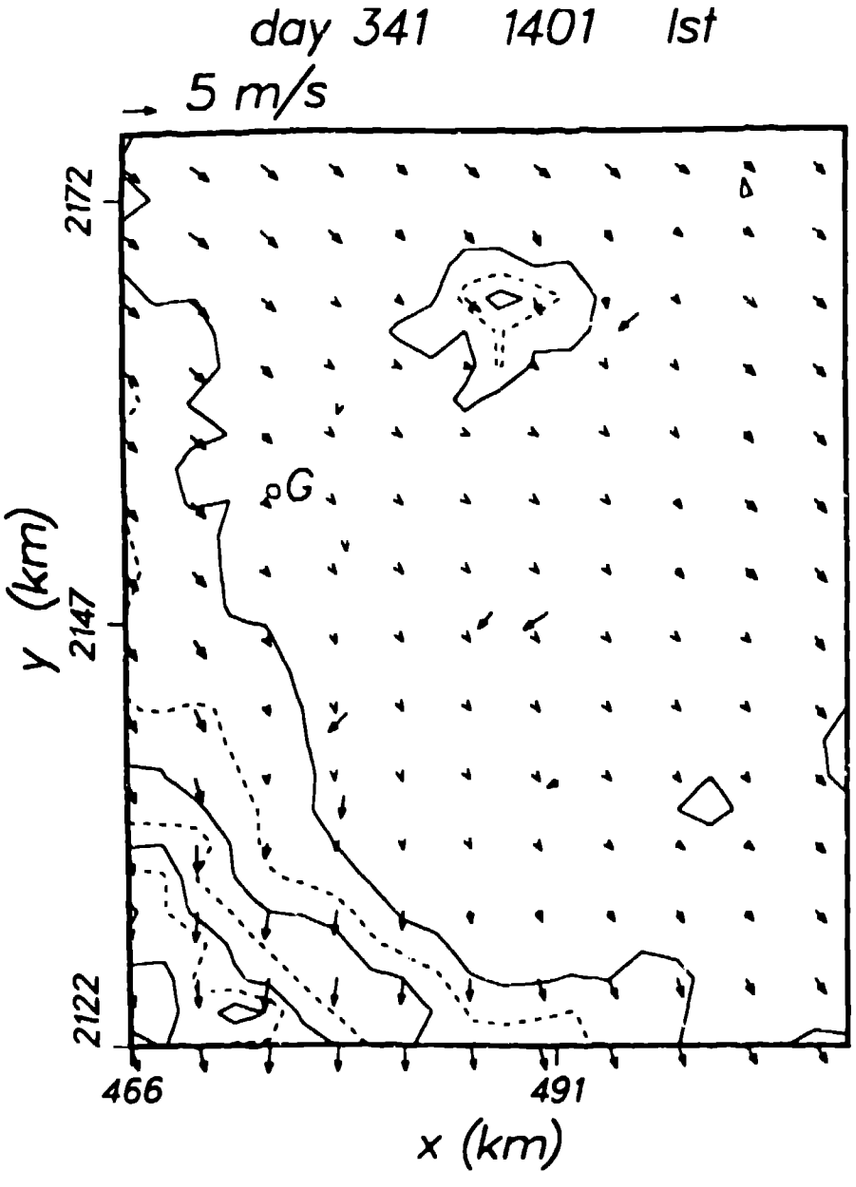

Figure 9: Modeled and measured 10 meter winds at 2 pm on December 7, 1987

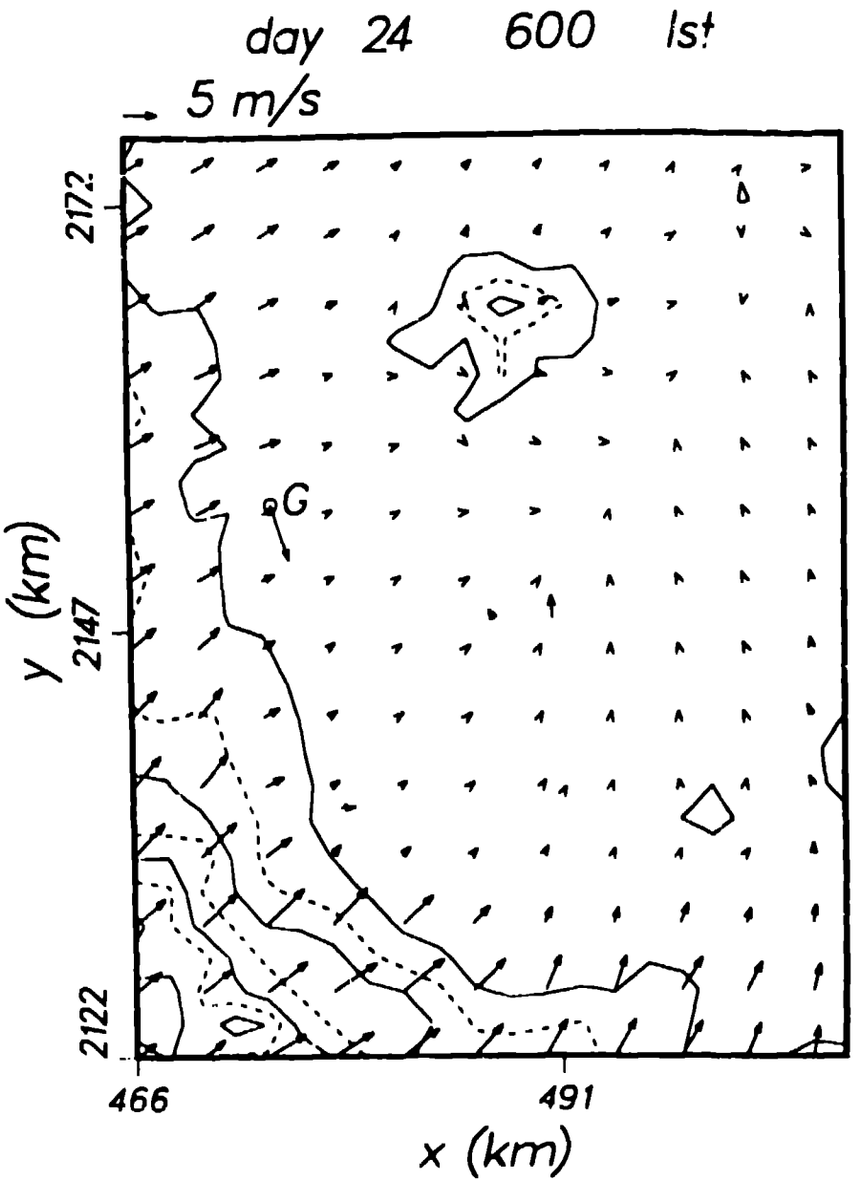

Figure 10: Modeled and measured 10 meter winds at 6 am on January 24 1988.

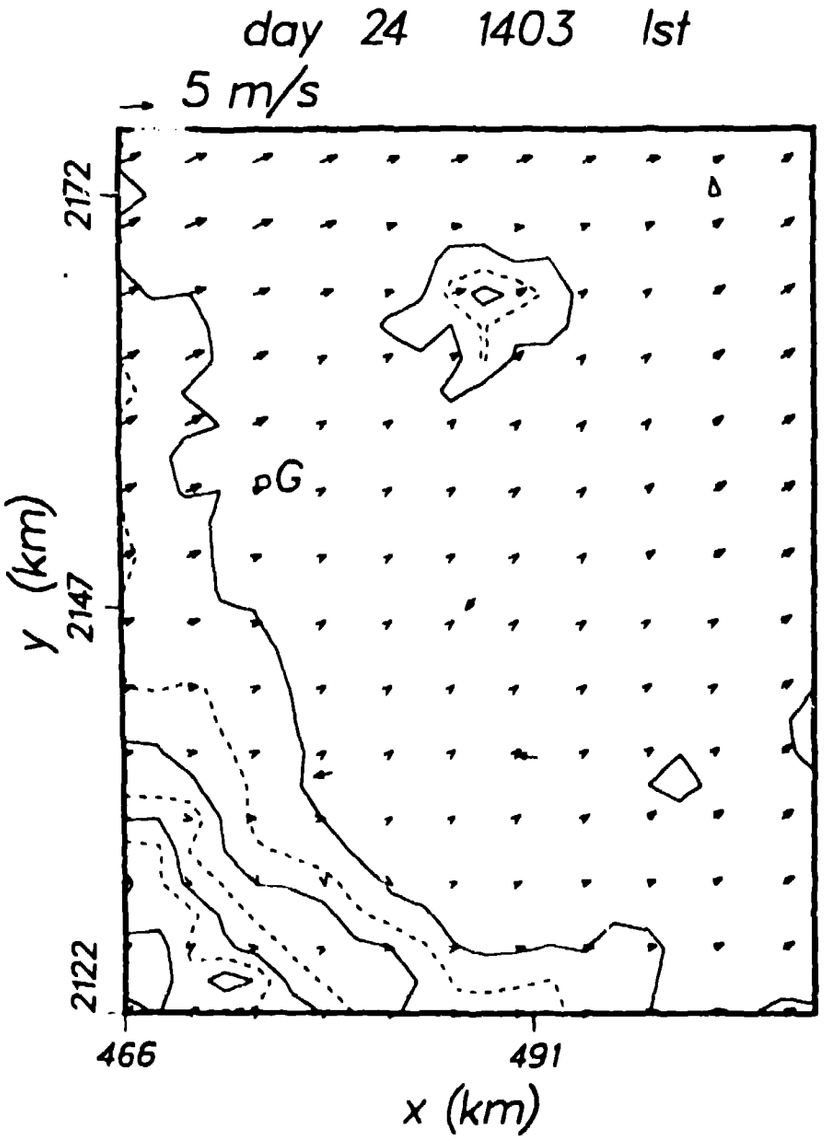

Figure 11: Modeled and measured 10 meter winds at 2 pm on January 24 1988.

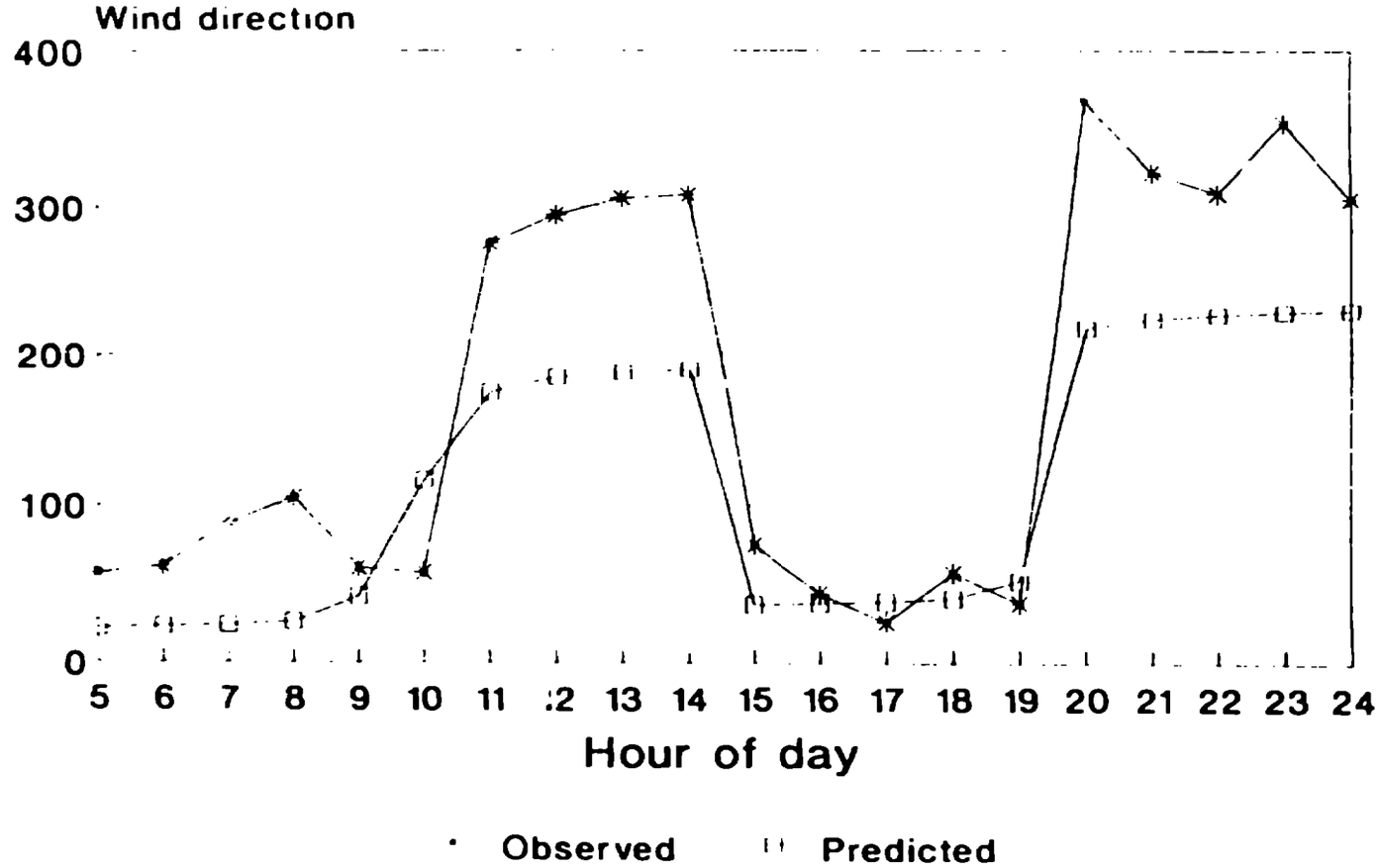

Figure 12: Modeled and observed wind directions at site T on the bad day.

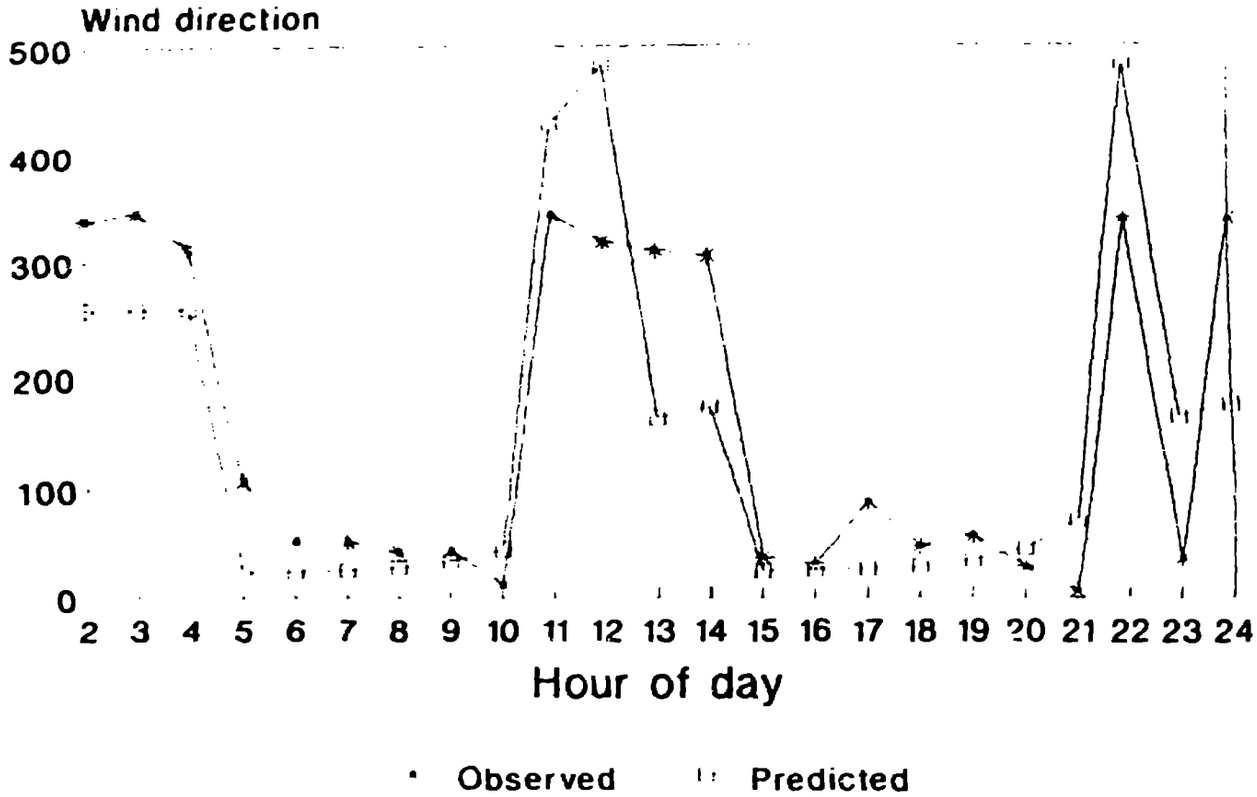

Figure 13: Modeled and observed wind directions at site Y on the bad day.

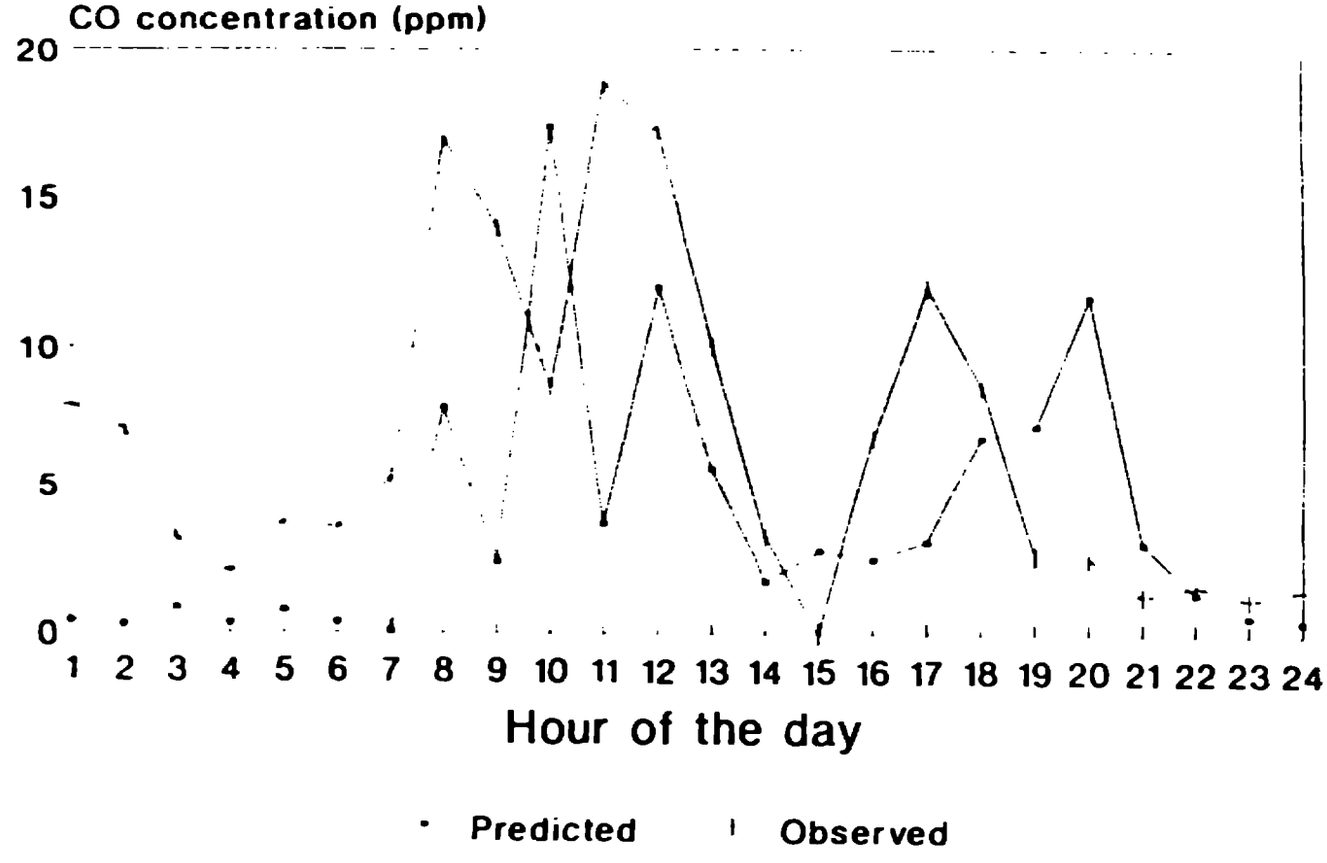

Figure 4. Modeled and observed co concentrations at site A on the bad day.

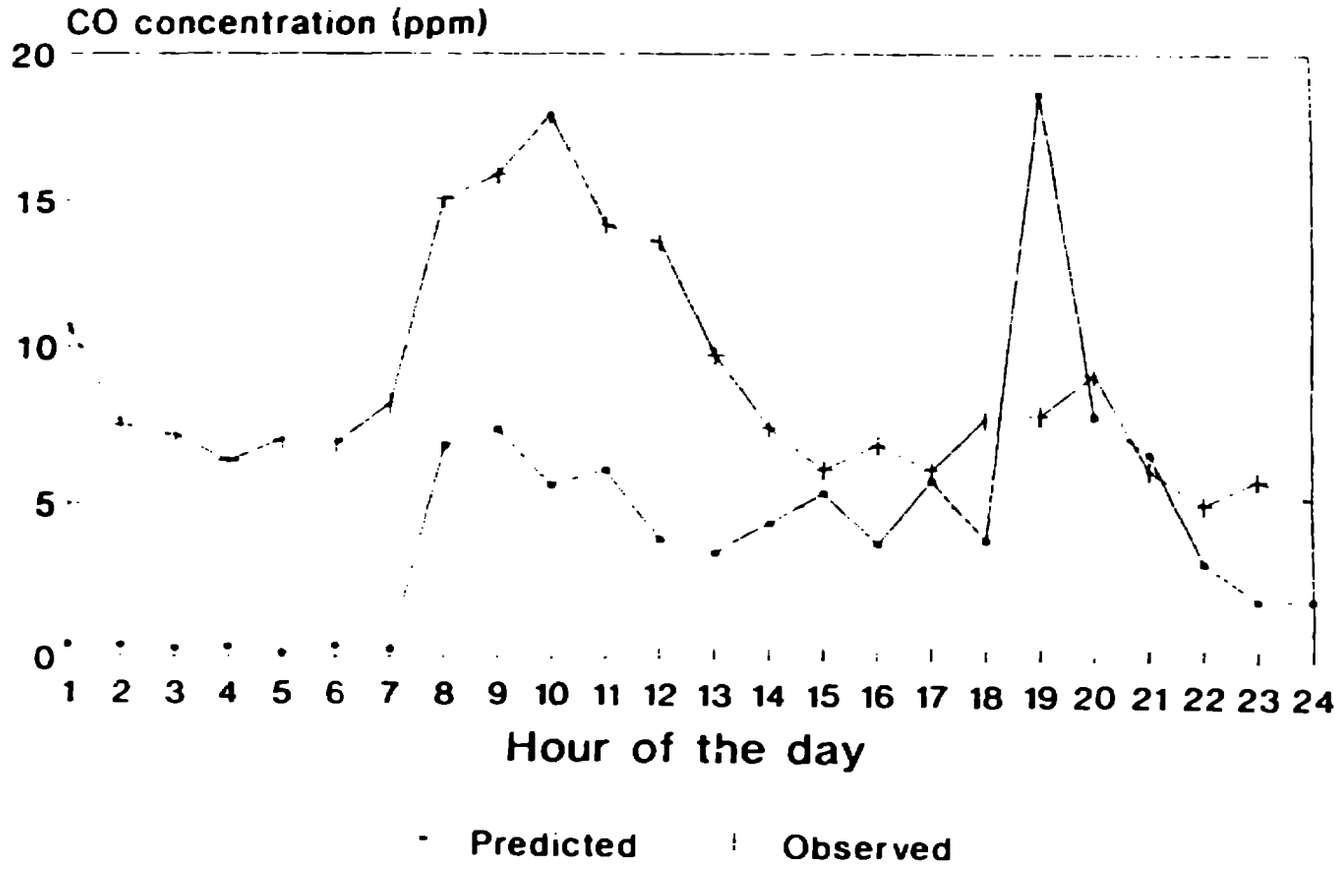

Figure 15: Modeled and observed co concentrations at site V on the bad day.